Simple and efficient method for functionalizing photocatalytic ceramic membranes and assessment of its applicability for wastewater treatment in up-scalable membrane reactors

Siwada Deepracha, Loubna Atfane, André Ayral, Makoto Ogawa

Simple and efficient method for functionalizing photocatalytic ceramic membranes and assessment of its applicability for wastewater treatment in up-scalable membrane reactors

Siwada Deepracha[a], Loubna Atfane[b], André Ayral[b], Makoto Ogawa[a,*]

[a]School of Energy Science and Engineering, Vidyasirimedhi Institute of Science and Technology (VISTEC), 555 Moo 1 Tumbol Payupnai, Amphoe Wangchan, Rayong 21210, Thailand

[b]Institut Européen des Membranes, IEM – UMR 5635, ENSAM, CNRS, Univ Montpellier, Montpellier, France

Corresponding Author

*E-mail: makoto.ogawa@vistec.ac.th

Abstract

A photocatalytically active layer composed of TiO_2 (Evonik P25) was successfully deposited on the macroporous (3 µm pore size) permeate side of an asymmetric porous alumina membrane with the aid of a smectite (a synthetic hectorite, Sumecton SWF) by dipping the membranes into an aqueous suspension containing P25 and the smectite. After the heat treatment at 400℃, the coated hybrid was adhered on the macroporous support enough to be applied for the photocatalytic decomposition of organics (methylene blue and phenol as model molecules) in water. The water permeance of the membranes after the coating with the P25-smectite hybrid was reduced by only 24% compared with that of the pristine membrane, showing that the advantages of the present method for the preparation of the photocatalyst layer on the surface of the macroporous alumina without significant infiltration of the suspension into the support pores. The amount of MB and phenol degraded using the P25-SWF hybrid was equal to 0.007 and 0.023 $mmol.L^{-1}$, respectively,

when the reaction was carried out using the four single-channel tubular membrane reactor at transmembrane pressures of 250 mbar. The implemented photocatalytic membrane reactor can easily be up-scaled by increase the size of the membrane module, with more tubes and longer tubes (lengths up to 1 m are commercially available), paving the way to potential technological applications for the continuous treatment of polluted waters.

Keywords: photocatalytic membrane; hybrid suspension; titania; smectite; organics photodegradation; wastewater treatment

1. Introduction

The deposition of semiconductor photocatalysts on solid supports has been extensively investigated to solve environmental problems (air and water contamination) by the photocatalytic decomposition of organic compounds in gas phase thanks to the unique characteristics of photocatalytic activity and superhydrophilicity induced by UV light irradiation [1-3] and that in aqueous solutions [4, 5]. Various wet (e.g. dip and spin coating from slurry and suspension) and dry processes (e.g. chemical vapor deposition and sputtering) have been employed to deposit semiconductor photocatalysts on supports [6-11]. Homogeneous coating of semiconductor photocatalysts has been obtained on flat and smooth surface of supports [12-14].

Photocatalytic membrane reactor is a hybrid process coupling the separation by membrane and the degradation by heterogeneous photocatalysis supported on the membrane. Ceramic membranes are advantageously used compared with organic polymer membranes considering the degradation of the polymers under UV exposure [15, 16]. Ceramic separation membranes usually possess asymmetric structures with thin separative layer and macroporous support providing the

required mechanical resistance. Depending on the membrane type, one or several intermediate layers are required between the separative layer and the macroporous support.

Semiconductor photocatalysts have been deposited as the separative layer or on the separative layer of alumina membranes with the average pore size in the range from 0.2 to 0.005 µm, corresponding to microfiltration or ultrafiltration membranes [17-20]. Both photocatalyst depositions on the macroporous support and the separative layer have also been reported [21-23]. Those membranes were used in applications of fouling prevention [24, 25]. TiO_2 was selected as a semiconductor photocatalyst due to potential to be used to construct photocatalytic membranes in water treatments [26-31]. Another option of photocatalytic membrane is to deposit photocatalysts on a macroporous support in contact with the permeate side, which is illuminated by UV light. An additional advantage of this configuration is to post-functionalize an existing membrane as photocatalyst contactor, without modifying its separative layer, and consequently its retention performance. Few studies have focused on the deposition of TiO_2 on macroporous alumina membrane supports (average pore size >3 µm) [32-34] because the deposition of photocatalytic layer homogeneously is difficult and infiltration of the photocatalysts inside the macropores occurs. These may cause an important loss of permeability.

Here, a new method is proposed to deposit semiconductor photocatalysts on porous supports, which is based on the simple addition of smectites in the suspension of TiO_2 particles and subsequent drying of the suspension on the porous support. Smectite (a group of clay minerals) is used as the additive in the present study, which acts as a rheology controlling agent to disperse TiO_2 in water and also acts as a binder upon solvent evaporation. Smectite has been used as an additive in paints due to its swelling properties by the expansion of the interlayer space in solvents (water and organic) [35]. The hybridization of TiO_2 with smectite for photocatalysts application

has been reported to modify the reactions and processes [36, 37]. Among available smectites, a synthetic hectorite (Sumecton SWF) was used because it is relatively pure for both phase and element (chemical formula; $Na_{0.3}(Mg,Li)_3Si_4O_{10}(OH)_2$) compared with natural smectites. The purity and finite particle size (less than 100 nm) of hectorite are important for the present study in order to minimize light scattering resulted from the particles and no un-wanted absorption of light by the impurities. Herein, the hectorite (Sumecton SWF) was chosen as the additive by taking advantages of the rheological and structural characteristics in order to deposit semiconductor photocatalysts (TiO_2 particles) on macroporous support for the construction of photocatalytic membranes.

The deposition of the photocatalyst layer was done by dipping flat or tubular macroporous alumina membranes into the aqueous suspension containing TiO_2 and the hectorite. The permeate flow measurements were performed for measuring the water permeability change of the membranes after their functionalization. The TiO_2-hectorite hybrid coated on the alumina support was applied as the photocatalytic membrane to assess the decomposition of organics (e.g. dye and phenol) in contaminated water.

2. Experimental

2.1.Materials

TiO_2 (Evonik P25) with the average primary particle size of 21 nm and the specific surface area (BET) of 50 ± 15 m^2/g was purchased from Aerosil Co., Ltd. A synthetic hectorite (Sumecton SWF) was kindly donated from Kunimine Industrial Co., Ltd. The cation exchange capacity of the hectorite is 70 mequiv/100 g of clay. Methylene blue and phenol were purchased from Aldrich Co., Ltd. All the chemicals were used without further purification.

The used alumina microfiltration membranes were supplied by Fraunhofer Institute for Ceramic Technologies and Systems (IKTS), Germany. They exhibited an asymmetric structure consisting of the macroporous support with the average pore size of 3 µm, the intermediate layer with the average pore size of 0.8 µm and the separative layer with the average pore size of 0.2 µm. Two types of membranes were used; (1) alumina disk with the diameter of 4.7 cm and the overall thickness of 1 mm and (2) alumina tube with the length of 20 cm, inner diameter of 0.7 cm and outer diameter of 1 cm, the separative layer being local in the internal side of the tube. Here, microfiltration membranes were selected because of their higher permeability compared with that of ultrafiltration or nanofiltration membranes with the same macroporous support while accompanying more intermediate layers and a mesoporous or microporous separative layer. Thus, the expected change of the water permeance before and after the coating is more important for microfiltration membranes.

2.2.Preparation and characterization of photocatalytic membrane

The photocatalytic membranes were prepared by dipping the alumina support into the aqueous suspension containing P25 and the hectorite (SWF) at 1 to 10 of SWF to P25 mass ratio with fixing the withdrawal rate of 1 $cm.min^{-1}$. In the case of the flat membrane, the side corresponding to the separative layer was temporary protected by a sticky film for avoiding any deposition or infiltration from that side during the dip-coating stage. For the tubular membranes, the tube ends were temporary closed for the same reason. After deposition, the functionalized membranes were dried at room temperature for one day and then thermally treated up to 400°C for one hour for mechanically stabilizing the deposit. Scanning electron microscope (SEM, S-4800 Hitachi) was used to observe the morphology of the deposited layer of hybrid on the alumina support. For some structural characterization, analogous powder sample was prepared by pouring

a hybrid suspension with the volume fraction of P25 in the suspension of 0.35 % in a beaker. Resulting powder after drying and heating at 400 °C was characterized by nitrogen adsorption-desorption at 77 K using an ASAP 2020 apparatus (Micromeritics). The sample was degassed at 250 °C under vacuum before the adsorption-desorption measurements. The mesopore size distribution was determined by the BJH method from the absorption isotherm. The mercury porosimetry (a model of Micromeritics' AutoPore IV 9500 Series) was also used to complete the porosity analysis of the hybrid powder.

2.3.Evaluation of the photocatalytic activity with the membrane reactors

The procedure to evaluate the performance of the photocatalytic membrane was previously developed where the photocatalytic performance was determined as the specific degradation rate, δ, corresponding to the number of mole of compound degraded by unit of membrane area and unit of time ($mol.m^{-2}s^{-1}$) [20, 30]. Briefly, the experiment was done by using the diffusion cell reactor (Figure 1), where the feed side was filled with the aqueous MB solution (concentration = 10^{-4} M), while the reception side was filled with pure water. The methylene blue (MB), used as a model molecule, was diffused from the feed side through the membrane (flat membrane coated on the permeate side with P25-SWF) and degraded at the permeate side, where the UV light was irradiated. The measured irradiance from the UV lamp on the functionalized side of the membrane was of 35 $W.m^{-2}$. The MB concentration in the reception tank was measured by colorimetry at wavelength = 664 nm.

The up-scalable membrane reactor (Figure 2) has specifically been developed in the present study for evaluating the reaction efficiency of the tubular membranes in the operation from the expectation to utilize in practical applications for wastewater treatment after up-scaling. The schematic diagram and the photographs of the designed membrane reactor are shown in Figure 2.

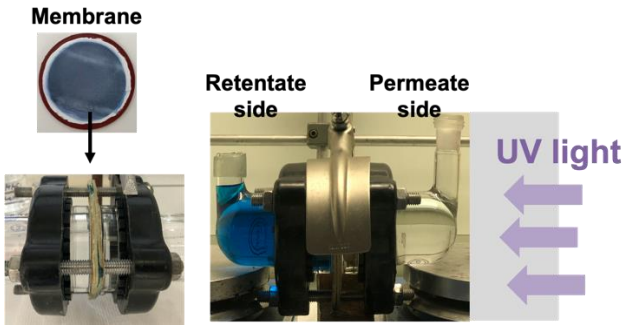

135 Figure 1. Diffusion cell used for measuring the degradation rate δ.

(a)

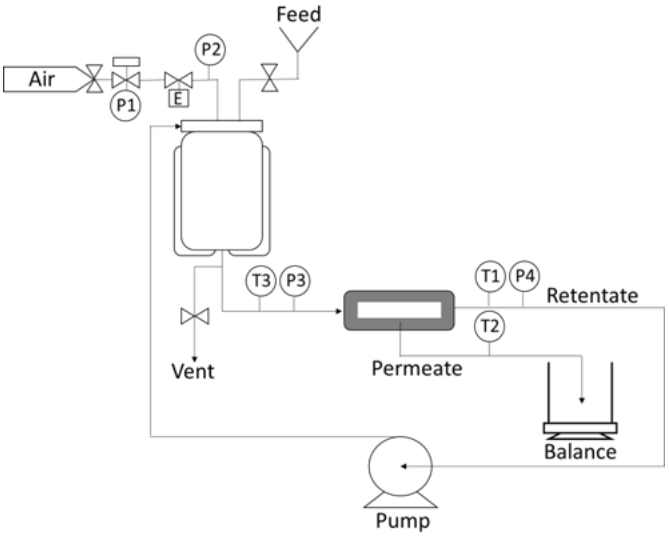

(b1)

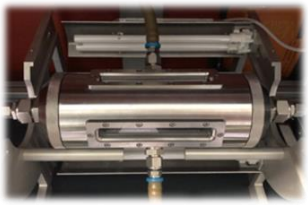

(b2)

(c)

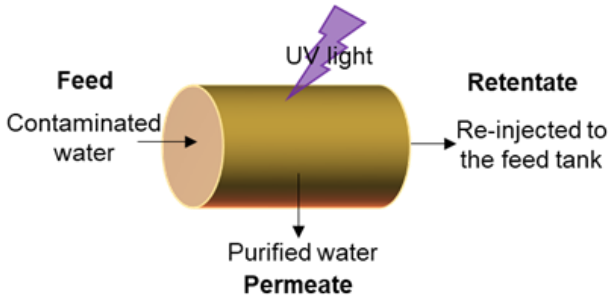

Figure 2. (a) Up-scalable membrane reactor used for testing the photocatalytic tubular membranes. Schematic representation of the overall pilot. (b1) and (b2) Filtration module equipped with four tubes with an effective length of 15.5 cm (overall filtration area of 136 cm^2), four borosilicate windows and four UV lamps. The central part in the module is especially machined for reflecting the light on the tube surfaces not directly accessible by the light beams of the UV lamps. (c) Schematic representation of the tubular membranes with tangential flow of the feed inside the tubes along the separative layer and the UV irradiation on the functionalized permeate side.

The maximum volume of solution filled in the feed tank is around 15 liters. The experiment was carried out by applying the transmembrane pressure of 0 – 2 bar using compressed air in the feed tank. The liquid velocity in the membrane loop was 1 $m.s^{-1}$. The solution at the retentate side was re-injected into the feed tank by the pump, while the solution at the permeate side was collected at the bottom part and weighted. The measured irradiance from the UV lamp on the functionalized side of the membrane was 100 $W{\cdot}m^{-2}$. The MB concentration in the permeate was measured by colorimetry at wavelength = 644 nm using JENWAY 7315 Spectrophotometer. The phenol concentration in the permeated was measured by liquid chromatography with a UV detector (Water 717 Autosample and Water 616 Pump with Water 2996 Photodiode Array Dectector and Thermo Scientific C18 L ¼ 150 mm, I.D. ¼ 4.6 mm column). The change of MB in the permeate without UV irradiation was examined as a control experiment to confirm the decomposition of

MB by P25 under the UV light. Gas chromatography coupled with mass spectrometry (GCMS) was used for detecting organic by-products resulting from the partial oxidation of phenol using Thermo Scientific TRACE 1300 and DSQ II with TG-5MS column. The adhesion of the hybrid layer supported on the support after the use for the reaction for two months was examined by SEM.

The amount of pure water diffused through the membranes was measured with operating time under different transmembrane pressures, ΔP. The plot of permeate flux J (defined by the volume of pure water at permeate side per unit time and unit of membrane area) versus applied transmembrane pressure (ΔP) for the heated pristine membrane was then drawn. The experiments were done in a cycle loop by increasing transmembrane pressure up to 2 bars, and subsequent decreasing it. The linear trendline was observed after the first cycle with the cyclic increasing and decreasing transmembrane pressure, which is referred to the reliability of the present reactor and operating system. This linear variation of the permeate flux with the transmembrane pressure is in agreement with the Darcy's law;

$$\text{Equation (1)}: \quad J = \frac{D}{\eta}.\frac{\Delta P}{L} = Pe.\Delta P$$

where J is permeate flux, η is dynamic viscosity of water, D is the intrinsic permeability of the porous membrane, L is the membrane thickness, ΔP is transmembrane pressure, and Pe is the water permeance.

The amount of MB degraded can be estimated from the specific degradation rate of MB determined in the diffusion cell reactor and the permeate flux at an applied transmembrane as following equation;

$$\text{Equation (2)}: \quad MB\ degraded = \frac{\delta}{Permeate\ flux}$$

3. Results and discussion

3.1.Functionalization of the alumina membranes

TiO_2 (P25, Evonik) was used as the photocatalyst for the construction of photocatalytic membrane due to its high efficiency for the photocatalytic decomposition of organics [38]. Without additive, the presence of P25 particles on the top surface of macroporous alumina support was observed after dipping the support into the P25 suspension (Figure 3a). On the other hand, when a smectite (synthetic hectorite; Sumecton SWF, hereafter abbreviated as SWF) was added into the P25 suspension, the homogeneously continuous layer of P25-SWF hybrid film was obtained on the macroporous alumina support (Figure 3b).

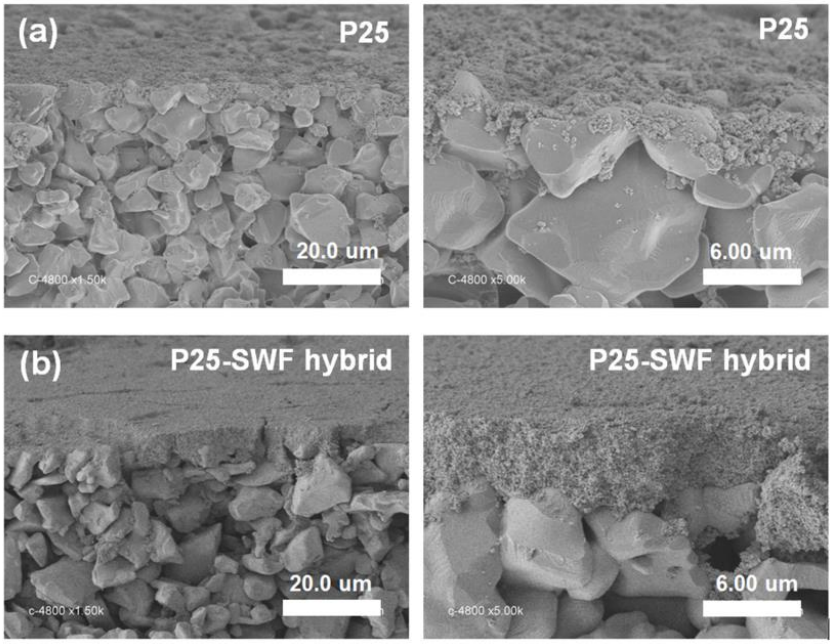

Figure 3. SEM images of (a) the P25 and (b) the P25-SWF hybrid at 1 to 10 of SWF to P25 mass ratio coated on porous alumina supports.

When SWF was added into the P25 suspension, the viscosity of the suspension increased because of the swelling of SWF. Thanks to the suspension stability, homogenous films of smectite

189 with various thicknesses have been prepared by drying the aqueous suspension of smectite on
190 supports [39, 40] as well as by other sophisticated methods including Langmuir-Blodgett [41] and
191 layer-by-layer deposition techniques [42, 43]. It is thought that the probability of the viscous
192 suspension containing P25 and SWF to be infiltrated into the pores of the membrane support was
193 lower than that of the P25 suspension without the addition of SWF, leading the homogeneous
194 coating of the hybrid layer on the macroporous alumina support after the drying.

195 The mass ratio of SWF to P25 was fixed at 1 (SWF) : 10 (P25) based on the previous

196 studies on the hybridization of TiO_2 and smectite film [44, 45], in which the optimum amount of
197 smectite in the hybrid was shown to depend on the particle size of TiO_2. Accordingly, the increase
198 of the SWF content was not examined further to control the viscosity of the suspension in the
199 present study. The volume fraction of P25 in the suspension varied to control the thickness of the
200 coating. The correlation between the thicknesses of P25-SWF hybrid coated on the porous alumina
201 support and the volume fraction of P25 in the suspension is shown in Figure 4. The thickness of
202 P25-SWF hybrid increased from 4 μm to 23 μm with increasing the volume fraction of P25 in the
203 suspension from 0.35 to 1.5 %. However, cracking at the surface was found for the coating from
204 0.75 % and 1.5 % of the volume fraction of P25 in the suspension giving rise to the thicker layers.
205 This phenomenon is due to the development of mechanical stresses across thick porous layers
206 during their drying [46].

207 The volume fraction of solids in the suspension (more than 40%) is required to achieve
208 high viscosity based on the theoretical prediction from a viscosity-concentration behavior [47].
209 Thanks to the smectite, the smaller amount of TiO_2 (0.35% of volume fraction of P25 in the
210 suspension) was enough to obtain the TiO_2 precursor for coating. The present methodology
211 provides an option to control viscosity of the suspension for coating the continuous layer of

semiconductor nanoparticles on the macroporous support thanks to the rheological characteristics (swelling properties in water) of smectites. In addition, the eco-friendly materials/method (non-toxic of smectite and no organic solvents for the preparation), as well as the thermal/chemical/mechanical resistances from the robustness of the inorganic-inorganic hybrids, are beneficial aspects for practical uses.

Based on the homogeneity with very limited cracking at the coating surface, the hybrid layer with thickness of 4 μm on the macroporous alumina, prepared at the volume fraction of P25 in the suspension of 0.35 %, was selected to examine the further experiment for evaluation of the photocatalytic efficiency in the membrane reactors. The equivalent powder was used for characterizing the pore size of this hybrid material. Broad pore size distribution in the range of few nm to a hundred nm with the maximum pore diameter of 70 nm was shown by the nitrogen adsorption-desorption isotherms. (The isotherms are shown in Figure S2.) The existence of such mesopores with the range of size distribution as well as the absence of the additional pores with larger size was confirmed by mercury porosimetry (Figure S3). The selection of microfiltration membranes was made to better estimate the change of permeability after coating. However, in order to avoid any damageable internal fouling of the membrane in operation, ultrafiltration and nanofiltration membranes (with an average pore size less than that of the photocatalytic layer, i.e. 70 nm) should be preferred. Such membranes exhibit much lower permeability thus limiting the contribution of the added active layer to the overall drop pressure across the membrane. Moreover, the developed method should easily be adapted for microfiltration membranes by adding pore-forming agents in the hybrid suspension in order to generate larger and interconnected pores in the deposited photocatalytic coating.

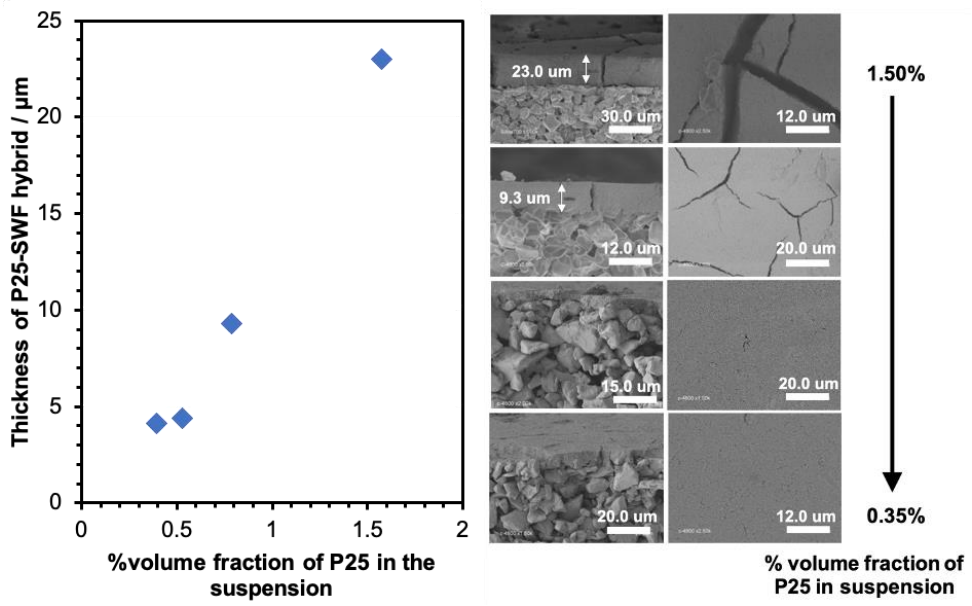

Figure 4. Correlation between the thicknesses of P25-SWF hybrid coated on the alumina versus %volume fraction of P25 in the suspension and the associated SEM images.

3.2 Assessment of the photocatalytic efficiency of the functionalized membranes

The efficiency of the layer of P25-SWF hybrid with thickness of 4 µm on a flat membrane was examined using the diffusion cell reactor, cyclic irradiation periods and by measuring the evolution of the MB concentration in the reception tank (Figure 5). The procedure to evaluate the efficiency of photocatalytic membrane was developed by conducting the degradation reaction of organic dissolved in water (methylene blue, MB commonly used as a model organic molecule) in the diffusion cell with two compartments separated by the membrane [20, 30]. The amount of a model organic (MB) degraded per unit area of photoactive surface and per unit time is defined as the specific degradation rate (δ). The evaluated specific degradation rate, δ, can be used in order to estimate the size and working conditions for further development on implementation of photocatalytic membranes in an up-scalable membrane reactor for practical application in wastewater purification.

The UV light was irradiated at the permeate side, where the layered hybrid of P25-SWF was coated on the alumina support. The specific degradation rate (δ) of MB using the P25-SWF hybrid was calculated to 2×10^{-8} mol.s^{-1}.m^{-2}. Despite the presence of photocatalytically inactive component (SWF), this value is comparable with the specific degradation rate of MB that was previously reported for other photocatalytic membranes (Table S1) [26, 48-50]. A decreased efficiency of the photocatalytic decomposition of stearic acid was observed when the SiO_2 was used as the binder to deposit TiO_2 on the support [51]. The pH of MB solution after the reaction was around 5, which indicated that the adsorption of MB on P25 and the alumina was not plausible because the surface of P25 and alumina are positively charged under the examined conditions. The decomposition of MB could be affected by the adsorption of MB on the smectite (SWF) because the enhanced decomposition of MB by the hybridization of smectite with TiO_2 as the hybrid film was previously reported [44], where the observed efficient decomposition was explained by the attractions between MB and P25.

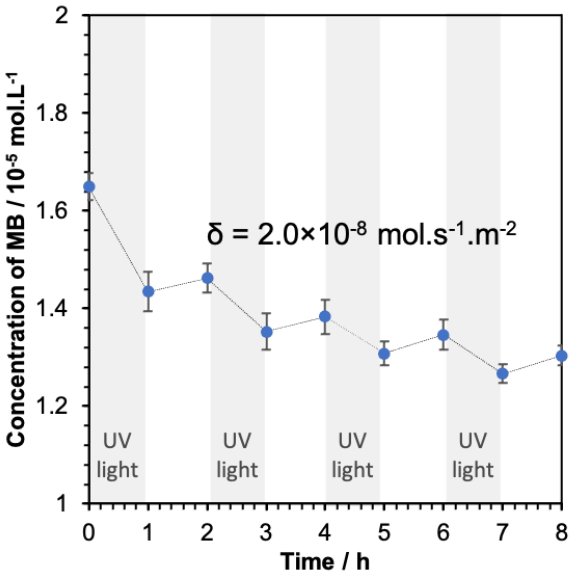

Figure 5. Photocatalytic decomposition of MB using the membrane of P25-SWF hybrid in the diffusion cell reactor.

3.3 Implementation of the up-scalable photocatalytic membrane reactor with four single-channel tubular membranes for wastewater purification

The suspension containing P25-SWF hybrid at 1 to 10 of SWF to P25 mass ratio was used to be coated on the permeate side of four tubular membranes. These membranes were placed in the membrane reactor in order to examine the decomposition of MB and phenol. The liquid velocity inside the loops being fixed at 1 $m.s^{-1}$, a turbulent flow was expected in the tubes from the estimation of Reynolds number (ca. 8000). The heat treatment of the pristine membranes under the identical conditions for the membranes coated with the hybrid was done to remove contaminants before measuring the permeate flux. The measured permeate flux of water for the membranes coated with the P25-SWF hybrid decreased if compared with that before the coating as shown in Figure 6a (red square). The water permeances were 182 and 138 $L.m^{-2}.h^{-1}.bar^{-1}$ for the membranes before and after the coating with the hybrid, respectively, as determined from the slope of the linear correlation. The intrinsic membrane permeability D for the membranes before and after the coating with the hybrid was determined to 1.52×10^{-15} and 1.16×10^{-15} m^2, respectively, using the Darcy's equation (equation 1).

The viscosity of the water flowed inside the tubular membrane is one of the parameters to affect the permeate flux. Viscosity of water strongly depends on temperature. The temperature of water at the permeate and retentate sides was measured during the operation, before and after UV irradiation in order to observe the change of permeate flux along the operation time (Figure 6b). The temperature of pure water at the retentate side (water flowing inside the tubular membrane) changed from 25 to 30^{o}C with longer operation time until 240 min. However, the permeate flux (slope of amount of water at permeate side versus time) was slightly changed from 22 to 24 $L.m^{-2}.h^{-1}$. So, the change of the permeate flux in longer operation time was not concerned.

Table 1 shows the reported water permeance using various TiO_2 based membranes. The significant decrease of the water permeance after the coating of TiO_2 on the separative layer (pore size < 0.2 µm) of the alumina membranes was observed [49, 52-55]. Permeability of membrane depends on the porosity of membrane. A significant loss of the permeability (40-80%) was previously observed, which was explained by the reduction of the porosity from plugging of TiO_2 into the pore of the alumina membranes. In contrast, a lower loss of water permeance (24%) was here observed for the hybrid coated on the macroporous alumina membrane. This indicates the advantage of the present method to coat TiO_2-based layer on the macroporous alumina support without important penalizing effects in terms of permeate flow decrease by minimizing the change of membrane porosity from the infiltration of the TiO_2 suspension into the pore of alumina. In addition, the role of the separative layer acting as the separation unit was not disturbed. Such a limited change of the permeability after the coating is beneficial in terms of process operation to reach the targeted permeate flux at low transmembrane pressure.

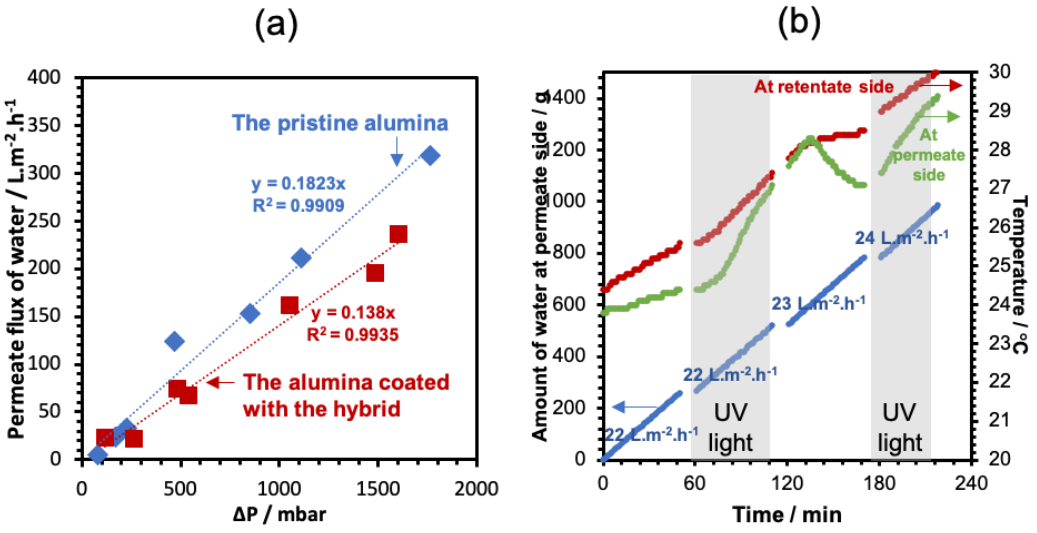

Figure 6. (a) Permeate flux of water for the membrane before and after coating with the P25-SWF hybrid under varied transmembrane pressures and (b) measured amount and temperature of water

after on and off cycle of UV irradiation for 1 h with fixing the transmembrane pressure at 125 mbar.

Table 1. Comparison of measured water permeance using different TiO_2 membranes.

Sample	Water permeance / $L.m^{-2}.h^{-1}.bar^{-1}$		Loss of water permeance (%)	Ref.
	Before coating	After coating		
TiO_2 film on alumina membrane (pore size = 0.2 µm) from commercial hydrosol S5-300B	1800	150	92	[49]
N doped TiO_2 film on alumina membrane (pore size = 0.2 µm)	3800	1600	58	[52]
TiO_2 film on alumina membrane (pore size = 0.1 µm)	11	6.71	39	[53]
Si doped TiO_2 film on alumina membrane (pore size = 0.1 µm)	1950	340	83	[54]
TiO_2 nanotube inside the alumina template (pore size = 0.2 µm)	40	5	88	[55]
P25-SWF hybrid coated on alumina membrane (pore size = 3 µm)	182	138	24	This work

Based on the previously estimated specific degradation rate of MB ($\delta = 2\times10^{-8}$ $mol.s^{-1}.m^{-2}$) using the P25-SWF hybrid in the diffusion cell reactor, the degraded amount of MB could be equal to 0.7 ppm (2.1×10^{-6} $mol.L^{-1}$) from the calculation using the equation (2) for an applied transmembrane of 250 mbar with the permeate flux of 34.5 $L.m^{-2}.h^{-1}$ (determined by the slope of the alumina coated with the hybrid in Figure 6a).

As shown in Figure 7a, the decrease of MB concentration at the feed tank from 9 ppm to 8 ppm at permeate before turning on the UV light may be explained by the adsorption of MB (positively charged dye) on the SWF (negatively charged layer). The decrease of MB concentration after turning on UV light in a cycle for 1 h from 8 to 6 ppm indicated that the MB was decomposed by the active species generated on P25 under the UV light irradiation. The degraded amount of MB after the UV irradiation for 1 h was equal to 2.1 ppm (6.4×10^{-6} $mol.L^{-1}$) when the reaction was conducted at transmembrane pressures of 250 mbar. The amount of MB

degraded in the up-scalable membrane reactor is thus higher than the expected amount of MB degraded from the estimation of the result in diffusion cell reactor (2.1×10^{-6} mol.L^{-1}). Efforts to use the similar emission spectra of the UV lamps (315-400 nm) in both diffusion cell and up-scalable membrane reactors have been made in order to minimize the effects of the different absorption of UV light by the P25 from the different wavelength. However, other factors such as irradiance and reaction conditions in both reactors were not identical to unable a direct comparison of the photocatalytic performance.

The linear relationship between the amount of MB degraded versus the permeate flux (Figure 7b) indicated that the MB decomposition depends on the probability of contact between MB molecule and active species created at the surface of the P25 nanoparticles. From the permeate flux of 34.5 L.m^{-2}.h^{-1} at the applied transmembrane pressure of 250 mbar and the thickness of the photocatalytic layer of 4 µm, the residence time of the MB molecules in this layer was calculated to be only 0.42 second. It must be added that only a few micrometers of the titania-based films, in depth from the UV-irradiated surface, are expected to be photocatalytically active [56]. Finally, the estimated size of the MB molecules (less than 2 nm) is very small in comparison with the pore size of the active layers (70 nm). All these factors can explain that only some part of the MB molecules crossing the membrane were photodegraded.

The photocatalytic reaction occurred without any loss the efficiency from leaching of the P25 particles from the alumina support, which referred to the adhesion of the continuous layer of P25-SWF hybrid with the alumina support was strongly enough for the reaction under operating conditions (applying transmembrane pressure). It is confirmed by the presence of similar thickness of layer of hybrid (4 µm) on the macroporous alumina support after use for two months in the membrane reactor, which is seen in the SEM images (Figure 7c).

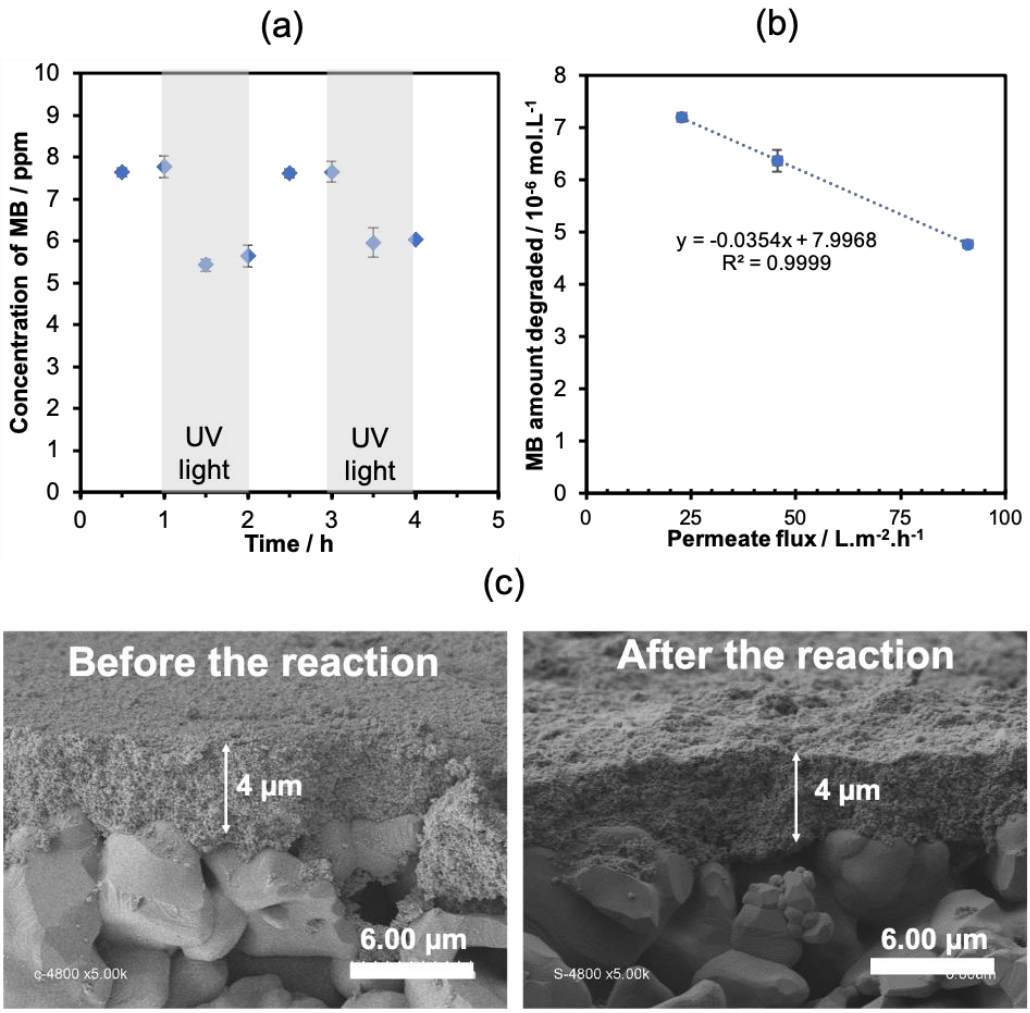

342

343 Figure 7. (a) MB concentration in the permeate with the photocatalytic membrane reactor working
344 at transmembrane pressure of 250 mbar and cyclic irradiation periods of one hour, (b) relationship
345 between the amount of MB degraded versus permeate flux and (c) SEM images of the hybrid on
346 alumina membrane before and after use for two months in the membrane reactor. The initial
347 concentration of MB in the feed tank is 3×10^{-5} mol.L^{-1} (9 ppm).

348 Phenol was selected as another model organic molecule in contaminated water. The
349 degraded amount of phenol after UV irradiation for 1 h was equal to 2.4 ppm, when the reaction
350 was conducted at the transmembrane pressures of 250 mbar (Figure 8a). Based on the previous

studies [49], the specific degradation rate using the diffusion reactor for MB and phenol was estimated at the similar value. The estimated value of specific degradation rate of phenol is assumed to be 2.1×10^{-6} mol.L^{-1} (0.2 ppm), which is very close to the degraded amount of phenol (2.4 ppm) observed at the transmembrane pressures of 250 mbar in the present study. Any organic by-products after the photodegradation of phenol using the P25-SWF hybrid were not detected in the permeate by GC-MS (Figure 8b). Phenol has been detected in groundwater (the range of 1 to 10 ppb), in rain (0.075–1.2 ppb), industrial rivers in the United States (5 ppb) [57], and in drinking water (0.5 ppb) according to EU directive [58]. The amount of phenol degraded at varied initial concentration of phenol in the feed was examined (Figure 8c). The experiment at very low concentration of phenol in ppb could not be done at present due to the detection limit (around 100 ppb) of the liquid chromatography. However, the mineralization of phenol contaminated in natural water may be possible because the higher percentage of phenol removal at lower initial concentration of phenol was observed (Figure 8d).

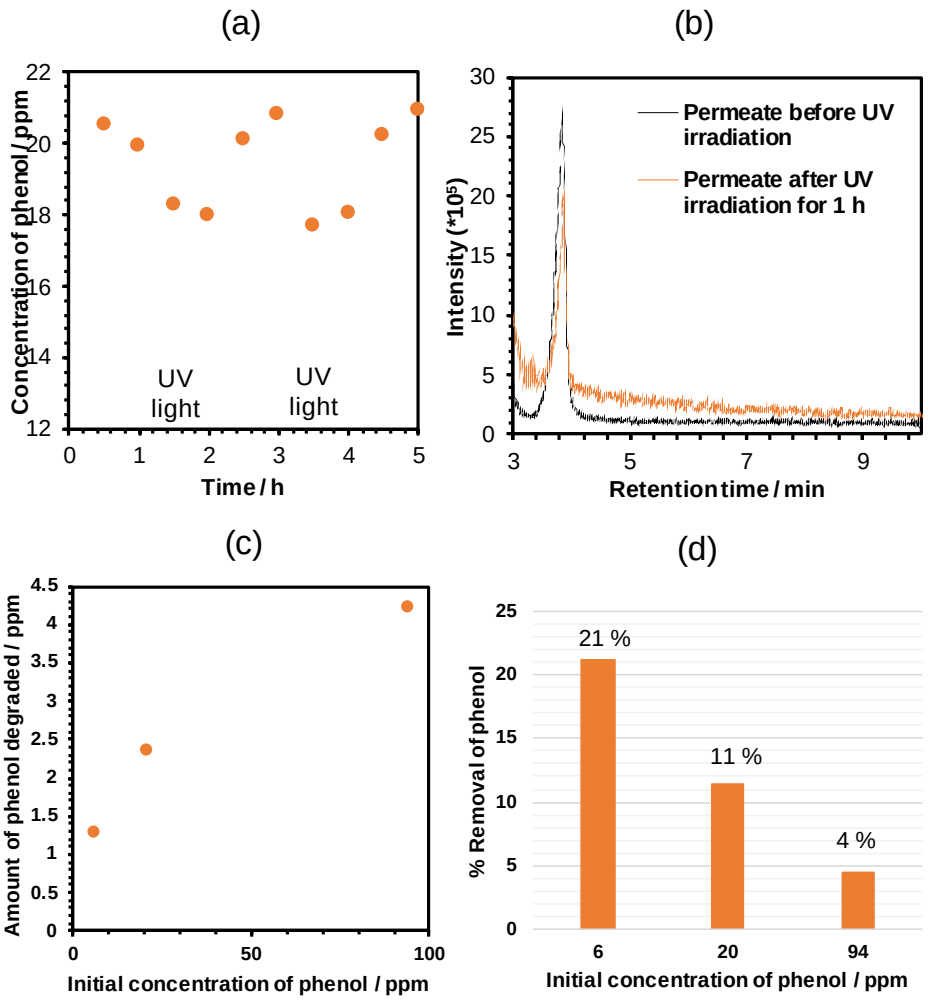

364

365 Figure 8. (a) Phenol concentration in the permeate with the photocatalytic membrane reactor
366 working at transmembrane pressure of 250 mbar and cyclic irradiation periods of one hour. (b)
367 GC-MS chromatogram of the solution before and after the reaction. The initial concentration of
368 phenol in the feed tank is 2.2×10^{-4} mol.L^{-1} (21 ppm). (c) Relationship between the amount of
369 phenol degraded and the initial concentration of phenol. (d) % Removal of phenol at different
370 initial concentrations of phenol.

371 Table 2 shows the reported efficiency of the photocatalytic phenol degradation using the
372 different types of photocatalysts deposited on membranes as supports. If compared with the

reported ones, the highest efficiency of phenol degradation is observed in the present study using the P25-SWF hybrid. It can be due to the homogenous deposited film formed with P25 titania nanoparticles known as a very efficient catalyst.

Furthermore, the implemented photocatalytic membrane reactor can be easily up-scaled by increase the size of the membrane module, with more tubes and longer tubes (lengths up to 1 m are commercially available), paving the way to potential technological applications for the continuous treatment of polluted waters.

4. Conclusions

The method to deposit a photocatalyst layer on a macroporous material with the aid of a smectite, was developed. By taking advantage of swelling properties of the smectite in water, the deposition of P25 and SWF hybrid was successfully achieved on the macroporous alumina support (3 µm pore size) without significant infiltration by dipping the alumina into the aqueous suspension containing P25 and SWF. The hybrid film (4 µm of thickness) coated on the porous alumina was used as the photocatalytic membrane to examine the decomposition of organics (e.g. dye and phenol) contaminated water using the membrane reactors. The amount of phenol degraded using the P25-SWF hybrid was equal to 0.023 $mmol.L^{-1}$, when the reaction was carried out using an easily up-scalable photocatalytic membrane reactor with four single-channel tubular membranes at transmembrane pressures of 250 mbar. The present method is applicable for the construction of photocatalytic ultrafiltration and nanofiltration ceramic membranes to be used for water polishing with in an up-scalable continuous flow membrane reactor.

Table 2. Photocatalytic degradation of phenol using the different photocatalysts deposited on supports as the photocatalytic membrane.

Sample	Preparation	Permeance ($L.m^{-2}.h^{-1}.bar^{-1}$)	Amount of phenol decomposed in an hour ($mmol.L^{-1}$)	Ref.
TiO_2 film on alumina membrane from commercial hydrosol S5-300B	Dipping the membrane into the aqueous suspension	150	0.0008	[49]
Carbon nitrile on polyethersulfone membrane	Drying the solution containing carbon nitrile and polymer to produce flat sheet membrane	264	0.006	[59]
TiO_2 deposited on polypropylene membrane	Immerging polypropylene into the dispersion of TiO_2	-	0.005	[60]
Carbon nitrile on hydrophilic surface modified polyethersulfone membrane	Drying the solution containing carbon nitrile and polymer to produce flat sheet membrane	22	0.006	[61]
P25-SWF hybrid coated on alumina membrane	Dipping the membrane into the aqueous suspension	138	0.023	This work

CRediT authorship contribution statement

Siwada Deepracha: Methodology, Formal analysis, Investigation, Writing – Original Draft, Writing – Review & Editing. **Loubna Atfane:** Methodology. **André Ayral:** Conceptualization, Validation, Formal analysis, Resources, Writing – Review & Editing. **Makoto Ogawa:** Conceptualization, Validation, Writing – Review & Editing, Supervision.

Declaration of Completing Interest

The authors declare that they have no known competing financial interests or personal relationships that could have appeared to influence the work reported in this paper.

Acknowledgements

This work was supported by the Research Chair Grant 2017 (grant number FDA-CO-2560-5655) from the National Science and Technology Development Agency (NSTDA), Thailand. One of the authors (S. Deepracha) acknowledges Vidyasirimedhi Institute of Science and Technology for the scholarship to his Ph.D. study. The authors would like to thank Mr. Bruno Navarra (IEM) for the help on technical support in operating with the membrane reactor, Mr. Didier Cot (IEM) for the help on SEM observation, Mr. Abdeslam El Manssouri (IEM) for the nitrogen adsorption-desorption analyses, Ms. Aline Gallitre (IEM) for the mercury porosimetry analyses, Mr. Eddy Petit (IEM) for the LC-UV analyses, and Mr. Guillaume Cazals (Plateforme Balard, LMP) for the GC-MS analyses.

Appendix A. Supplementary data

N_2 adsorption-desorption isotherms and BJH pore size distribution of the equivalent powder of hybrid. The pore size distribution of the equivalent powder of hybrid observed by mercury porosimetry.

References

1. D. Wood, S. Shaw, T. Cawte, E. Shanen, B. Van Heyst, An overview of photocatalyst immobilization methods for air pollution remediation, Chem. Eng. J. (2019) 123490.

2. R. Wang, K. Hashimoto, A. Fujishima, M. Chikuni, E. Kojima, A. Kitamura, M. Shimohigoshi, T. Watanabe, Light-induced amphiphilic surfaces, Nature 388 (6641) (1997) 431-432.

3. H. Choi, S.R. Al-Abed, D.D. Dionysiou, Nanostructured titanium oxide film-and membrane-based photocatalysis for water treatment, Nanotechnology applications for clean water, William Andrew, New York, 2009, pp. 39-46.

4. A.Y. Shan, T.I.M. Ghazi, S.A. Rashid, Immobilization of titanium dioxide onto supporting materials in heterogeneous photocatalysis: a review, Appl. Catal. A-Gen. 389 (1-2) (2010) 1-8.

5. M. Sheikh, M. Pazirofteh, M. Dehghani, M. Asghari, M. Rezakazemi, C. Valderrama, J.L. Cortina, Application of ZnO nanostructures in ceramic and polymeric membranes for water and wastewater technologies: a review, Chem. Eng. J. (2019) 123475.

6. G. Balasubramanian, D.D. Dionysiou, M.T. Suidan, I. Baudin, J.M. Laıné, Evaluating the activities of immobilized TiO_2 powder films for the photocatalytic degradation of organic contaminants in water, Appl. Catal. B 47 (2) (2004) 73-84.

7. J. Shang, W. Li, Y. Zhu, Structure and photocatalytic characteristics of TiO_2 film photocatalyst coated on stainless steel webnet, J. Mol. Catal A-Chem. 202 (1-2) (2003) 187-195.

8. J.G. Yu, H.G. Yu, B. Cheng, X.J. Zhao, J.C. Yu, W.K. Ho, The effect of calcination temperature on the surface microstructure and photocatalytic activity of TiO_2 thin films prepared by liquid phase deposition, J. Phys. Chem. B 107 (50) (2003) 13871-13879.

9. A. Mills, N. Elliott, I.P. Parkin, S.A. O'Neill, R.J. Clark, Novel TiO_2 CVD films for semiconductor photocatalysis, J. Photochem. Photobio. A 151 (1-3) (2002) 171-179.

10. J. Lim, C. Lee, Effects of substrate temperature on the microstructure and photoluminescence properties of ZnO thin films prepared by atomic layer deposition, Thin Solid Films 515 (7-8) (2007) 3335-3338.

11. N. Lehraki, M.S. Aida, S. Abed, N. Attaf, A. Attaf, M. Poulain, ZnO thin films deposition by spray pyrolysis: Influence of precursor solution properties, Curr. Appl. Phys. 12 (5) (2012) 1283-1287.

12. E. González, A. Bonnefond, M. Barrado, A.M.C. Barrasa, J.M. Asua, J.R. Leiza, Photoactive self-cleaning polymer coatings by TiO_2 nanoparticle Pickering miniemulsion polymerization, Chem. Eng. J. 281 (2015) 209-217.

13. L. Cordero-Arias, S. Cabanas-Polo, H. Gao, J. Gilabert, E. Sanchez, J.A. Roether, D.W. Schubert, S. Virtanen, A.R. Boccaccini, Electrophoretic deposition of nanostructured-TiO_2/chitosan composite coatings on stainless steel, RSC adv. 3 (28) (2013) 11247-11254.

14. T. Kamegawa, Y. Shimizu, H. Yamashita, Superhydrophobic surfaces with photocatalytic self-cleaning properties by nanocomposite coating of TiO_2 and polytetrafluoroethylene, Adv. Mater. 24 (27) (2012) 3697-3700.

15. S.H. Kim, S.Y. Kwak, B.H. Sohn, T.H. Park, Design of TiO_2 nanoparticle self-assembled aromatic polyamide thin-film-composite (TFC) membrane as an approach to solve biofouling problem, J. Membr. Sci. 211 (1) (2003) 157-165.

16. H. Song, J. Shao, Y. He, B. Liu, X. Zhong, Natural organic matter removal and flux decline with PEG–TiO_2-doped PVDF membranes by integration of ultrafiltration with photocatalysis, J. Membr. Sci. 405 (2012) 48-56.

17. H. Zhang, X. Quan, S. Chen, H. Zhao, Fabrication and characterization of silica/titania nanotubes composite membrane with photocatalytic capability, Environ. Sci. Technol. 40 (19) (2006) 6104-6109.

18. H. Choi, E. Stathatos, D.D. Dionysiou, Sol–gel preparation of mesoporous photocatalytic TiO_2 films and TiO_2/Al_2O_3 composite membranes for environmental applications, Appl. Catal. B 63 (1-2) (2006) 60-67.

19. F. Bosc, A. Ayral, C. Guizard, Mesoporous anatase coatings for coupling membrane separation and photocatalyzed reactions, J. Membr. Sci. 265 (1-2) (2005) 13-19.

20. C.P. Athanasekou, G.E. Romanos, F.K. Katsaros, K. Kordatos, V. Likodimos, P. Falaras, Very efficient composite titania membranes in hybrid ultrafiltration/photocatalysis water treatment processes, J. Membr. Sci. 392 (2012) 192-203.

21. G.E. Romanos, C.P. Athanasekou, F.K. Katsaros, N.K. Kanellopoulos, D.D. Dionysiou, V. Likodimos, P. Falaras, Double-side active TiO_2-modified nanofiltration membranes in continuous flow photocatalytic reactors for effective water purification, J. Hazard. Mater. 211 (2012) 304-316.

22. G.E. Romanos, C.P. Athanasekou, V. Likodimos, P. Aloupogiannis, P. Falaras, Hybrid ultrafiltration/photocatalytic membranes for efficient water treatment, Ind. Eng. Chem. Res. 52 (39) (2013) 13938-13947.

23. N.G. Moustakas, F.K. Katsaros, A.G. Kontos, G.E. Romanos, D.D. Dionysiou, P. Falaras, Visible light active TiO_2 photocatalytic filtration membranes with improved permeability and low energy consumption, Catal. Today 224 (2014) 56-69.

24. C. Li, W. Sun, Z. Lu, X. Ao, C. Yang, S. Li, Systematic evaluation of TiO_2-GO-modified ceramic membranes for water treatment: Retention properties and fouling mechanisms, Chem. Eng. J. 378 (2019) 122138.

25. X. Zhang, T. Zhang, J. Ng, D.D. Sun, High-performance multifunctional TiO_2 nanowire ultrafiltration membrane with a hierarchical layer structure for water treatment, Adv. Funct. Mater. 19 (23) (2009) 3731-3736.

26. Z. Song, M. Fathizadeh, Y. Huang, K.H. Chu, Y. Yoon, L. Wang, W.L. Xu, M. Yu, TiO_2 nanofiltration membranes prepared by molecular layer deposition for water purification, J. Membr. Sci. 510 (2016) 72-78.

27. A. Ayral, Ceramic membranes photocatalytically functionalized on the permeate side and their application to water treatment, Membranes 9 (5) (2019) 64.

28. H. Choi, A.C. Sofranko, D.D. Dionysiou, Nanocrystalline TiO_2 photocatalytic membranes with a hierarchical mesoporous multilayer structure: synthesis, characterization, and multifunction, Adv. Funct. Mater. 16 (8) (2006) 1067-1074.

29. B.J. Starr, V.V. Tarabara, M. Herrera-Robledo, M. Zhou, S. Roualdès, A. Ayral, Coating porous membranes with a photocatalyst: Comparison of LbL self-assembly and plasma-enhanced CVD techniques, J. Membr. Sci. 514 (2016) 340-349.

30. R. Ahmad, J.K. Kim, J.H. Kim, J. Kim, Well-organized, mesoporous nanocrystalline TiO_2 on alumina membranes with hierarchical architecture: Antifouling and photocatalytic activities, Catal. Today 282 (2017) 2-12.

31. B. Bayati, Y. Bayat, N. Charchi, M. Ejtemaei, A.A. Babaluo, M. Haghighi, E. Drioli, Preparation of crack-free nanocomposite ceramic membrane intermediate layers on α-alumina tubular supports, Sep. Sci. Technol. 48 (13) (2013) 1930-1940.

32. M. Zhou, S. Roualdes, A. Ayral, New photocatalytic contactors obtained by PECVD deposition of TiO_2 thin layers on the surface of macroporous supports, Eur. Phys. J. Spec. Top. 224 (9) (2015) 1871-1882.

511 33. C.P. Athanasekou, S. Morales-Torres, V. Likodimos, G.E. Romanos, L.M. Pastrana-
512 Martinez, P. Falaras, D.D. Dionysiou, J.L. Faria, J.L. Figueiredo, A.M. Silva, Prototype composite
513 membranes of partially reduced graphene oxide/TiO_2 for photocatalytic ultrafiltration water
514 treatment under visible light, Appl. Catal. B 158 (2014) 361-372.
515 34. E. Luster, D. Avisar, I. Horovitz, L. Lozzi, M.A. Baker, R. Grilli, H. Mamane, N-doped
516 TiO_2-coated ceramic membrane for carbamazepine degradation in different water
517 qualities, Nanomaterials 7 (8) (2017) 206.
518 35. F. Bergaya, B.K.G. Theng, G. Lagaly, Handbook of Clay Science, Elsevier Science, The
519 Netherlands, 2006.
520 36. S. Deepracha, K. Vibulyaseak, M. Ogawa, Complexation of TiO_2 with clays and clay
521 minerals for hierarchically designed functional hybrids, Advanced Supramolecular
522 Nanoarchitectonics, William Andrew, New York, 2019, pp. 125-150.
523 37. E. Ruiz-Hitzky, P. Aranda, M. Akkari, N. Khaorapapong, M. Ogawa, Photoactive
524 nanoarchitectures based on clays incorporating TiO_2 and ZnO nanoparticles, Beilstein J.
525 Nanotechnol. 10 (1) (2019) 1140–1156.
526 38. U.I., Gaya, A.H. Abdullah, Heterogeneous photocatalytic degradation of organic
527 contaminants over titanium dioxide: a review of fundamentals, progress and problems, J.
528 Photochem. Photobiol. C 9 (1) (2008) 1-12.
529 39. N.A. Kotov, T. Haraszti, L. Turi, G. Zavala, R.E. Geer, I. Dekany, J.H. Fendler,
530 Mechanism of and defect formation in the self-assembly of polymeric polycation−montmorillonite
531 ultrathin films, J. Am. Chem. Soc. 119 (29) (1997) 6821-6832.
532 40. M. Ogawa, M. Takahashi, C. Kato, K. Kuroda, Oriented microporous film of
533 tetramethylammonium pillared saponite, J. Mater. Chem. 4 (4) (1994) 519-523.

41. K. Inukai, Y. Hotta, S. Tomura, M. Takahashi, A. Yamagishi, Preparation of the Langmuir− Blodgett film of a clay−alkylammonium adduct and its use as a barrier for interlayer photoinduced electron transfer, Langmuir 16 (20) (2000) 7679-7684.

42. Y. Zhou, Z. Li, N. Hu, Y. Zeng, J.F. Rusling, Layer-by-layer assembly of ultrathin films of hemoglobin and clay nanoparticles with electrochemical and catalytic activity, Langmuir 18 (22) (2002) 8573-8579.

43. C.H. Zhou, Z.F. Shen, L.H. Liu, S.M. Liu, Preparation and functionality of clay-containing films, J. Mater. Chem. 21 (39) (2011) 15132-15153.

44. S. Deepracha, S. Bureekaew, M. Ogawa, Synergy effects of the complexation of a titania and a smectite on the film formation and its photocatalyst'performance, Appl. Clay Sci. 169 (2019) 129-134.

45. T. Goto, M. Ogawa, Visible-light-responsive photocatalytic flow reactor composed of titania film photosensitized by metal complex-clay hybrid, ACS Appl. Mater. Inter. 7 (23) (2015) 12631-12634.

46. C.J. Brinker, G.W. Scherer, Sol-gel science: the physics and chemistry of sol-gel processing, Elsevier, Academic press, United States, 2013.

47. R.J. Farris, Prediction of the viscosity of multimodal suspensions from unimodal viscosity data, Trans. Soc. Rheol. 12 (2) (1968) 281-301.

48. L. Naszályi, F. Bosc, A. El Mansouri, A. Van Der Lee, D. Cot, Z. Hórvölgyi, A. Ayral, Sol–gel-derived mesoporous SiO_2/ZnO active coating and development of multifunctional ceramic membranes, Sep. Purif. Technol. 59 (3) (2008) 304-309.

555 49. L. Djafer, A. Ayral, A. Ouagued, Robust synthesis and performance of a titania-based
556 ultrafiltration membrane with photocatalytic properties, Sep. Purif. Technol. 75 (2) (2010) 198-
557 203.
558 50. F. Bosc, A. Ayral, P.A. Albouy, C. Guizard, A simple route for low-temperature synthesis
559 of mesoporous and nanocrystalline anatase thin films, Chem. Mater. 15 (12) (2003) 2463-2468.
560 51. F. Bosc, A. Ayral, C. Guizard, Mixed TiO_2–SiO_2 mesostructured thin films, Thin Solid
561 Films 495 (1-2) (2006) 252-256.
562 52. R. Grilli, D. Di Camillo, L. Lozzi, I. Horovitz, H. Mamane, D. Avisar, M.A. Baker, Surface
563 characterisation and photocatalytic performance of N-doped TiO_2 thin films deposited onto 200
564 nm pore size alumina membranes by sol–gel methods, Mater. Chem. Phys. 159 (2015) 25-37.
565 53. H. Choi, E. Stathatos, D.D. Dionysiou, Photocatalytic TiO_2 films and membranes for the
566 development of efficient wastewater treatment and reuse systems, Desalination 202 (1-3) (2007)
567 199-206.
568 54. N. Ma, X. Quan, Y. Zhang, S. Chen, H. Zhao, Integration of separation and photocatalysis
569 using an inorganic membrane modified with Si-doped TiO_2 for water purification, J. Membr.
570 Sci. 335 (1-2) (2009) 58-67.
571 55. X. Zhang, A.J. Du, P. Lee, D.D. Sun, J.O. Leckie, Grafted multifunctional titanium dioxide
572 nanotube membrane: separation and photodegradation of aquatic pollutant, Appl. Catal. B 84 (1-
573 2) (2008) 262-267.
574 56. D. Chen, F. Li, A.K. Ray, Effect of mass transfer and catalyst layer thickness on
575 photocatalytic reaction, AIChE J. 46 (5) (2000) 1034-1045.

576 57. J. Crawford, O. Faroon, F. Llados, J.D. Wilson, Toxicological Profile for Phenol. Atlanta,
577 GA: US Department of Health and Human Services, Public Health Service, Agency for Toxic
578 Substances and Disease Registry, 2008.
579 58. J. Kochana, J. Adamski, A. Parczewski, A critical view on the phenol index as a measure
580 of phenol compounds content in waters. Application of a biosensor, Ecol. Chem. Eng. S 19 (3)
581 (2012) 383-391.
582 59. N.E. Salim, N.A.M. Nor, J. Jaafar, A.F. Ismail, T. Matsuura, M.R. Qtaishat, M.H.D.
583 Othman, M.A. Rahman, F. Aziz, N. Yusof, Performance of PES/LSMM-OGCN Photocatalytic
584 Membrane for Phenol Removal: Effect of OGCN Loading, Membranes 8 (3) (2018) 42.
585 60. S. Yang, J. S. Gu, H.Y. Yu, J. Zhou, S.F. Li, X.M. Wu, L. Wang, Polypropylene membrane
586 surface modification by RAFT grafting polymerization and TiO_2 photocatalysts immobilization
587 for phenol decomposition in a photocatalytic membrane reactor, Sep. Purif. Technol. 83 (2011)
588 157-165.
589 61. N.E. Salim, J. Jaafar, A.F. Ismail, M.H.D. Othman, M.A. Rahman, N. Yusof, M. Qtaishat,
590 T. Matsuura, F. Aziz, W.N.W. Salleh, Preparation and characterization of hydrophilic surface
591 modifier macromolecule modified poly (ether sulfone) photocatalytic membrane for phenol
592 removal, Chem. Eng. J. 335 (2018) 236-247.